AIAA JOURNAL
Vol. 39, No. 10, October 2001

Wall-Normal-Free Reynolds-Stress Closure for Three-Dimensional Compressible Separated Flows

G. A. Gerolymos* and I. Vallet†
Université Pierre-et-Marie-Curie, 91405 Orsay, Paris, France

A near-wall Reynolds-stress closure that is independent of the distance from the wall and of the normal to the wall direction is developed and validated. Particular attention was given in the applicability of the model to complex three-dimensional flows with shock waves and boundary-layer separation. In the separated flow region, measurements and model computations indicate that the flatness parameter A of the anisotropy tensor a_{ij} approaches unity. Therefore, control of separation is achieved in the model through the particular functional dependence of the rapid pressure–strain isotropization of production model coefficient on A. Echo terms are treated by replacing geometric normals and distances by functions of the gradients of turbulence length scale and anisotropy tensor invariants. The model is initially compared with measurements for compressible flat-plate boundary-layer flows. It is then validated by comparison with experimental data in a two-dimensional compression corner oblique shock-wave/boundary-layer interaction at Mach 3. Finally the model is applied to the computation of the three-dimensional interaction of a Mach 1.5–1.8 strong shock wave with the boundary layers of a rectangular channel fitted with a swept bump on the lower wall, and results are compared with measurements. One important advantage of the proposed model is its robustness in complex three-dimensional flows. A detailed discussion of the range of validity of the model and possible improvements is presented.

Introduction

REYNOLDS-STRESS models (RSM) offer definite advantages over eddy-viscosity models, which are pathologically wrong in many situations, especially for configurations with strong secondary flows or with system rotation effects.[1–6] The use of near-wall terms has made these models independent of particular law-of-the-wall forms.[7–11] Recently it has been recognized that for the computation of complex flows it is important to use models independent of such geometric parameters as the distance from the wall n or the normal to the wall direction $\boldsymbol{e}_n = n_i \boldsymbol{e}_i$. It must be stressed that in several instances, such as three-dimensional flow in the vicinity of solid corners[12] or flow through the tip-clearance gap of turbomachinery rotors,[13] these parameters are defined in a completely arbitrary manner.[14]

Durbin[15,16] has proposed a methodology based on the solution of a Poisson equation for the inhomogeneity effects on dissipation and redistribution terms. This method has been successfully applied to several incompressible flow configurations.[15–17] The main drawbacks of this approach are 1) the need to solve one field equation per Reynolds-stress component at each flow solver iteration and 2) the difficulty in specifying boundary conditions for the Poisson equations in complex three-dimensional configurations (the boundary conditions are dependent on the component considered relatively to the normal to the wall direction, resulting in coupling between the Poisson equations in an arbitrary coordinate system not aligned with the solid boundaries).

Djenidi and Antonia[18] developed a model specific to flat-plate boundary-layer flows that used many ad hoc assumptions but did not contain wall-reflection terms (the normal to the wall direction was, however, present in the dissipation tensor modeling strategy). More recently, So and Yuan[19] developed a geometry-independent near-wall Reynolds-stress closure that uses a quadratic pressure–strain closure without echo terms. The normal-free near-wall behavior of the model is achieved through the ε equation and the ε_{ij} tensor. The model has been applied to three-dimensional developing flow in a square duct[19] and to two-dimensional backstep flow.[20] Shima[21] developed a model completely independent of n and $\boldsymbol{e}_n$ that does not contain wall-echo redistribution terms. This model was applied to several accelerated and decelerated boundary-layer flows and showed encouraging general agreement with measurements. The strategy adopted was to use quasi-linear models for the pressure–strain terms, with no echo terms. The functional dependence of the model coefficients (especially of the slow terms) on the anisotropy tensor invariants[22] A and A_2 and on the turbulence Reynolds number Re_T is used to mimic the echo effect. The anisotropy tensor and its invariants are defined from the Reynolds-stress tensor $\widetilde{u_i'' u_j''}$ and the turbulence kinetic energy $k = \frac{1}{2}\widetilde{u_i'' u_i''}$:

$$a_{ij} = \widetilde{u_i'' u_j''}/k - \tfrac{2}{3}\delta_{ij}, \qquad A_1 = a_{ii} = 0, \qquad A_2 = a_{ik}a_{ki}$$

$$A_3 = a_{ik}a_{kj}a_{ji}, \qquad A = \left[1 - \tfrac{9}{8}(A_2 - A_3)\right] \tag{1}$$

Launder and Li[14] did not use echo terms by adopting a cubic model for the redistribution terms and using effective velocity gradients, following a suggestion by Bradshaw et al.[23] that points out the inaccuracy of taking out the mean-flow velocity gradients, of the volume integral for pressure–strain in inhomogeneous flow. The effective velocity gradients include a second derivative correction in the direction of the flow inhomogeneity, which is estimated by taking the gradient of functions of the turbulence length scale ℓ_T and the anisotropy-tensor invariants[22] A and A_2. Although this technique yields too stiff a model for complex three-dimensional configurations containing large three-dimensional strains, it introduces the idea of using such gradients to determine the normal to the wall direction in the echo terms.[24–26] This technique of using echo terms but with a pseudonormal direction that mimics correctly the echo directionality has been adopted in the present work, but with the further improvement of separating the unit's pseudonormal determining gradients from the value of the echo-terms coefficients.

There are few published papers dealing with near-wall Reynolds-stress work in the compressible (transonic and supersonic) flow regime. Sommer et al.[27,28] have developed a closure for the Reynolds stresses coupled to transport equations for the temperature fluctuation and its dissipation, and applied it to zero-pressure-gradient flat-plate supersonic boundary-layer flows. A linear pressure–strain model was used. Ladeinde[29] also used a linear pressure–strain model to compute the interaction of a supersonic boundary layer with a continuous compression wave generated by concave surface curvature. Gerolymos and Vallet[12] used a compressible extension of the

Received 24 December 1999; revision received 22 January 2001; accepted for publication 7 March 2001.

*Professor, Director, Laboratoire d'Energétique, Unité Associée au Centre National de Recherche Scientifique, Bâtiment 511.

†Assistant Professor, Laboratoire d'Energétique, Unité Associée au Centre National de Recherche Scientifique, Bâtiment 511.

near-wall model of Launder–Shima[30] (quasi-linear pressure–strain closure) to compute three-dimensional shock-wave/boundary-layer interaction in a square channel fitted with a swept bump on the lower wall. To obtain a numerically stable model, the authors had to replace the transport equation for the dissipation rate ε with a transport equation for the modified dissipation $\varepsilon^* = \varepsilon - 2\check{\nu}[\text{grad}\sqrt{k}]^2$ based on the k–ε model of Launder–Sharma[31] because of the much more stable wall boundary condition $\varepsilon^*_w = 0$ (Ref. 12). Comparison with measurements was satisfactory, but the model systematically underestimates separation. Batten et al.[26] used a nonlinear model for both the slow pressure–strain terms ϕ_{ij1} and for the rapid pressure–strain terms ϕ_{ij2}. A cubic model was used for ϕ_{ij2} resulting in a near-wall model of rather overwhelming complexity. The model was applied to the computation of two-dimensional shock-wave/boundary-layer interactions and to the three-dimensional interaction of a supersonic flow with a cylindrical fin. These authors also used a transport equation for the modified dissipation rate ε^*.

There are mainly two families of near-wall RSMs: those based on linear or quasi-linear pressure–strain closures[30,32–36] and those based on quadratic or cubic closures for the rapid terms ϕ_{ij2} (Refs. 14 and 24–26). The quasi-linear models are very robust.[12] The use of complex cubic ϕ_{ij} models in real three-dimensional configurations with shock-wave/boundary-layer interactions at solid corners is not an easy task. To the authors knowledge, no such work has been reported (the computations of Batten et al.[26] deal with a shock wave detached in front of a cylinder). In general, nonlinear models for ϕ_{ij2} have been fine tuned to reproduce complex details of simple shear flows and as a result contain an oversensitive dependence on such parameters[25] as the nondimensional strain S_{RNG} and vorticity Ω_{RNG} that will go off bounds in complex three-dimensional separated shock-wave/boundary-layer interactions. The use of these parameters is, in the authors' opinion, an unwise choice because (with the exception of simple shear flows such as two-dimensional boundary layers, jets, and wakes) they do not vary within a known range (as do the anisotropy-tensor invariants[22] $A \in [0,\ 1]$ and $A_2 \in [0,\ \frac{8}{3}]$). In the case of rotating pipe flow, Pettersson et al.[17] encountered serious problems with cubic models for ϕ_{ij2} and concluded that "highly nonlinear (cubic) pressure–strain models fail severely."

The purpose of the present work is to develop a near-wall RSM along the following ideas: 1) provide a completely wall-normal-free formulation, 2) use a dissipation equation based on ε^* for computational robustness, 3) use modified quasi-linear models for ϕ_{ij1} and ϕ_{ij2} that will improve the results obtained by the Launder–Shima–Sharma closure (see Ref. 12) in separated flows, 4) include echo terms based on pseudonormals both for ϕ_{ij1} and ϕ_{ij2}, 5) systematically avoid the use of S_{RNG} and Ω_{RNG}, and 6) ensure robustness of the model in complex three-dimensional shock-wave/boundary-layer interactions.

Model Development

Mean Flow

The flow is modeled by the compressible Favre–Reynolds-averaged three-dimensional Navier–Stokes equations[12]

$$\frac{\partial \bar{\rho}}{\partial t} + \frac{\partial \bar{\rho}\tilde{u}_\ell}{\partial x_\ell} = 0 \tag{2}$$

$$\frac{\partial \bar{\rho}\tilde{u}_i}{\partial t} + \frac{\partial}{\partial x_\ell}[\bar{\rho}\tilde{u}_i\tilde{u}_\ell + \bar{p}\delta_{i\ell}] - \frac{\partial}{\partial x_\ell}[\bar{\tau}_{i\ell} - \bar{\rho}\widetilde{u_i''u_\ell''}] = 0 \tag{3}$$

$$\frac{\partial}{\partial t}[\bar{\rho}\check{h}_t - \bar{p}] + \frac{\partial \bar{\rho}\tilde{u}_\ell\check{h}_t}{\partial x_\ell} - \frac{\partial}{\partial x_\ell}[\tilde{u}_i(\bar{\tau}_{i\ell} - \bar{\rho}\widetilde{u_i''u_\ell''}) - (\bar{q}_\ell + \bar{\rho}\widetilde{h''u_\ell''})] = S_{\check{h}_t} \tag{4}$$

where t is the time, x_ℓ are the Cartesian space coordinates, u_i are the velocity components, ρ is the density, p is the pressure, δ_{ij} is the Kronecker symbol, τ_{ij} are the viscous stresses, and $(\tilde{\cdot})$ indicates Favre averaging, $(\bar{\cdot})$ nonweighted averaging, $(\cdot'')$ Favre fluctuations, and $(\cdot')$ nonweighted fluctuations (for any flow quantity b: $\tilde{b} + \underline{b''} = \bar{b} + \underline{b'}$ and $\underline{\overline{b''}} = \bar{b} - \tilde{b}$, and for any flow quantities[37] b_1 and b_2: $\underline{b_1''b_2'} \equiv \underline{b_1'b_2'} \equiv \underline{b_1'b_2''}$). Also, $\check{h}_t = \tilde{h} + \frac{1}{2}\tilde{u}_i\tilde{u}_i$ is the total enthalpy of the mean flow (which is different from the Favre-averaged total enthalpy $\tilde{h}_t = \tilde{h} + \frac{1}{2}\tilde{u}_i\tilde{u}_i + \text{k} = \check{h}_t + k$), h is the specific enthalpy, and $k = \frac{1}{2}\widetilde{u_i''u_i''}$ is the turbulence kinetic energy. The $(\check{\cdot})$ is used to denote a function of average quantities that is neither a Favre average nor a nonweighted average. The source term in the mean energy equation is[12]

$$S_{\check{h}_t} = -\left(P_k - \bar{\rho}\varepsilon + \overline{p'\frac{\partial u_\ell''}{\partial x_\ell}}\right) + \frac{\partial}{\partial x_\ell}[\overline{pu_\ell''}] + (-\bar{p}\delta_{i\ell} + \bar{\tau}_{i\ell})\frac{\partial \overline{u_i''}}{\partial x_\ell} \tag{5}$$

where $P_k = \frac{1}{2}P_{\ell\ell}$ is the turbulence kinetic energy production (equal to the trace of the Reynolds-stresses production tensor P_{ij}) and ε is its dissipation. In the present work we preferred to define the turbulent heat flux as an enthalpy transport $\bar{\rho}\widetilde{h''u_i''}$, as will be discussed in the heat-flux closure section. This involves including a pressure diffusion term to $S_{\check{h}_t}$ compared to previous work of the authors.[12] The mean viscous stresses are approximated in the usual way by[37–39]

$$\bar{\tau}_{ij} \cong \check{\mu}\left(\frac{\partial \tilde{u}_i}{\partial x_j} + \frac{\partial \tilde{u}_j}{\partial x_i} - \frac{2}{3}\frac{\partial \tilde{u}_\ell}{\partial x_\ell}\delta_{ij}\right), \qquad \bar{q}_i \cong -\check{\kappa}\frac{\partial \tilde{T}}{\partial x_i} \tag{6}$$

and the thermodynamics of the working gas are approximated by[40]

$$\bar{p} = \bar{\rho}R_g\tilde{T} = \bar{\rho}\frac{\gamma - 1}{\gamma}\tilde{h}$$

$$\check{\mu} = \mu(\tilde{T}) = \mu_{273}\frac{\tilde{T}^{\frac{3}{2}}}{273.15^{\frac{3}{2}}}\frac{T_S + 273.15}{T_S + \tilde{T}}$$

$$\check{\kappa} = \kappa(\tilde{T}) = \kappa_{273}\frac{\mu(\tilde{T})}{\mu_{273}}[1 + A_\kappa(\tilde{T} - 273.15)] \tag{7}$$

where γ is the isentropic exponent, R_g the gas constant, μ the dynamic viscosity, and κ the heat conductivity. For air $R_g = 287.04\ \text{m}^2 \cdot \text{s}^{-2} \cdot \text{K}^{-1}$, $\gamma = 1.4$, $\mu_{273} = 17.11 \times 10^{-6}\ \text{Pa} \cdot \text{s}$, $\kappa_{273} = 0.0242\ \text{W} \cdot \text{m}^{-1} \cdot \text{K}^{-1}$, $T_S = 110.4\ \text{K}$, and $A_\kappa = 0.00023\ \text{K}^{-1}$.

Turbulent Heat Flux

Several authors define the turbulent heat flux as internal-energy transport,[29,41] whereas others prefer to consider enthalpy transport.[37] This is a matter of definition, and when pressure diffusion $\underline{p'u_i''}$ and density fluctuation effects $\underline{u_i''}$ are neglected, both definitions are equivalent. They introduce, however, a different relation between temperature transport and heat flux and, as a consequence, a different functional dependence on the isentropic exponent. Defining the turbulent heat flux as enthalpy transport recovers the correct incompressible limit of the temperature equation and was, therefore, preferred. In the present work the turbulent heat flux is closed by a simple gradient model[37–40]:

$$\bar{\rho}\widetilde{h''u_i''} = -\frac{\mu_T c_p}{Pr_T}\frac{\partial \tilde{T}}{\partial x_i}, \qquad c_p = \frac{\gamma}{\gamma - 1}R_g, \qquad \mu_T = C_\mu\check{\mu}Re_T^*$$

$$C_\mu = 0.09\exp\left[-\frac{3.4}{\left(1 + 0.02Re_T^*\right)^2}\right], \qquad Re_T^* = \frac{\bar{\rho}k^2}{\check{\mu}\varepsilon^*} \tag{8}$$

where c_p is the heat capacity at constant pressure, Pr_T the turbulent Prandtl number, and Re_T^* the turbulence Reynolds number based on the modified dissipation ε^*. In the present work $Pr_T = 0.9$ to obtain the correct recovery temperature for turbulent flow over an adiabatic wall.[37]

Reynolds-Stress Transport

The transport equations for the Favre–Reynolds-averaged Reynolds stresses are[42]

$$\underbrace{\frac{\partial \bar\rho \widetilde{u_i'' u_j''}}{\partial t} + \frac{\partial}{\partial x_\ell}(\bar\rho \widetilde{u_i'' u_j''} \tilde u_\ell)}_{\text{convection } C_{ij}}$$

$$= \underbrace{\frac{\partial}{\partial x_\ell}(-\bar\rho \widetilde{u_i'' u_j'' u_\ell''} - \overline{p' u_j''}\delta_{i\ell} - \overline{p' u_i''}\delta_{j\ell} + \overline{u_i'' \tau_{j\ell}' + u_j'' \tau_{i\ell}'})}_{\text{diffusion } d_{ij}}$$

$$+ \underbrace{\overline{p'\left(\frac{\partial u_i''}{\partial x_j} + \frac{\partial u_j''}{\partial x_i} - \frac{2}{3}\frac{\partial u_k''}{\partial x_k}\delta_{ij}\right)}}_{\text{redistribution } \phi_{ij}}$$

$$+ \underbrace{\left(-\bar\rho \widetilde{u_i'' u_\ell''}\frac{\partial \tilde u_j}{\partial x_\ell} - \bar\rho \widetilde{u_j'' u_\ell''}\frac{\partial \tilde u_i}{\partial x_\ell}\right)}_{\text{production } P_{ij}}$$

$$- \underbrace{\overline{\left(\tau_{j\ell}'\frac{\partial u_i''}{\partial x_\ell} + \tau_{i\ell}'\frac{\partial u_j''}{\partial x_\ell}\right)}}_{\text{dissipation } \bar\rho\varepsilon_{ij}} + \underbrace{\frac{2}{3}\overline{p'\frac{\partial u_k''}{\partial x_k}}\delta_{ij}}_{\text{pressure–dilatation}}$$

$$+ \underbrace{\left(-\overline{u_i''}\frac{\partial \bar p}{\partial x_j} - \overline{u_j''}\frac{\partial \bar p}{\partial x_i} + \overline{u_i''}\frac{\partial \bar\tau_{j\ell}}{\partial x_\ell} + \overline{u_j''}\frac{\partial \bar\tau_{i\ell}}{\partial x_\ell}\right)}_{\text{density fluctuation effects } K_{ij}} \tag{9}$$

Convection C_{ij} and production P_{ij} are exact terms. The modeling concerning the remaining terms is discussed in the following subsections.

Compressibility Terms

Although effects of compressibility are present in some of the flows studied, it was felt during the development of the model that it would be difficult to optimize them without previously developing and extensively validating (in a wide Mach number range) a baseline model that would neglect them. This would avoid the danger of using compressibility terms closures to correct other errors of the model. In the present work, direct compressibility effects K_{ij}, pressure–dilatation correlation, and pressure diffusion are neglected:

$$K_{ij} \cong 0, \qquad \overline{p'\frac{\partial u_\ell''}{\partial x_\ell}} \cong 0, \qquad \overline{p u_\ell''} \cong 0$$

$$\overline{u_i''} \cong 0, \qquad S_{\tilde h_t} \cong -(P_k - \rho\varepsilon) \tag{10}$$

Dissipation

To avoid the instability associated with the wall boundary condition $\varepsilon_w = 2\breve\nu_w(\partial\sqrt{k}/\partial n)^2$, a compressible flow extension to the Launder–Sharma[31] equation for the modified dissipation rate of the turbulence kinetic energy,

$$\varepsilon^* = \varepsilon - 2\breve\nu\left(\text{grad}\sqrt{k}\right)^2, \qquad \bar\rho\breve\nu = \breve\mu \tag{11}$$

for which the wall boundary condition is $\varepsilon_w^* = 0$, was used. The transport equation is the same as the one used in the Launder–Sharma k–ε^* turbulence closure[31] (also see Ref. 38), with the exception of the diffusion term, where a tensorial diffusion coefficient is used, as is usual in Reynolds-stress closures.[14,29,43] The modeled form of the equation is[12]

$$\frac{\partial \bar\rho\varepsilon^*}{\partial t} + \frac{\partial}{\partial x_\ell}\left(\tilde u_\ell \bar\rho\varepsilon^*\right) - \frac{\partial}{\partial x_\ell}\left[\left(\breve\mu\delta_{k\ell} + C_\varepsilon\frac{k}{\varepsilon^*}\bar\rho\widetilde{u_k'' u_\ell''}\right)\frac{\partial \varepsilon^*}{\partial x_k}\right]$$

$$= C_{\varepsilon 1}P_k\frac{\varepsilon^*}{k} - C_{\varepsilon 2}\bar\rho\frac{\varepsilon^{*2}}{k} + \frac{2\breve\mu\mu_T}{\bar\rho}(\nabla^2\,\tilde{\boldsymbol{V}})^2 \tag{12}$$

$$C_\varepsilon = 0.18, \qquad C_{\varepsilon 1} = 1.44, \qquad C_{\varepsilon 2} = 1.92\left(1 - 0.3e^{-Re_T^{*2}}\right) \tag{13}$$

This is of course a baseline equation, and the authors are aware that further work is needed on the dissipation equation. However, as noted by Hanjalić,[11] the effort should be concentrated on improving the reattachment behavior and not viscous-sublayer details in near-zero pressure-gradient flows.

Diffusion

Because pressure diffusion is neglected, diffusion is approximated by

$$d_{ij} \cong \frac{\partial}{\partial x_k}\left[-\bar\rho\widetilde{u_i'' u_j'' u_k''} + \breve\mu\frac{\partial \widetilde{u_i'' u_j''}}{\partial x_k}\right] \tag{14}$$

where the triple correlations are modeled following Hanjalić and Launder[44]

$$\widetilde{u_i'' u_j'' u_k''} \cong -C_s\frac{k}{\varepsilon}\left[\widetilde{u_i'' u_\ell''}\frac{\partial \widetilde{u_j'' u_k''}}{\partial x_\ell} + \widetilde{u_j'' u_\ell''}\frac{\partial \widetilde{u_k'' u_i''}}{\partial x_\ell} + \widetilde{u_k'' u_\ell''}\frac{\partial \widetilde{u_i'' u_j''}}{\partial x_\ell}\right]$$

$$C_s = 0.11 \tag{15}$$

Preliminary tests for shock-wave/boundary-layer interactions showed little difference in the results when using the Hanjalić–Launder[44] model compared to the simpler Daly–Harlow model,[45] used by Gerolymos and Vallet.[12] The Hanjalić–Launder[44] model was as a consequence preferred because it respects the tensorial symmetry of the triple velocity correlations $\widetilde{u_i'' u_j'' u_k''}$ (Refs. 8 and 11).

Pressure–Strain Redistribution

The pressure–strain redistribution term augmented by the dissipation tensor anisotropy[30] is split into the slow and rapid parts and the corresponding echo terms:

$$\phi_{ij} - \bar\rho\left(\varepsilon_{ij} - \tfrac{2}{3}\delta_{ij}\varepsilon\right) = \phi_{ij1} + \phi_{ij1}^w + \phi_{ij2} + \phi_{ij2}^w \tag{16}$$

The pressure–strain redistribution terms ϕ_{ij} are the most important item in the closure because they control both the separation and the reattachment processes.

The slow part ϕ_{ij1} is modeled by a simple quasi-linear return to isotropy model whose coefficient has been optimized by Launder and Shima[30] to account also for the anisotropic part of the dissipation tensor $\varepsilon_{ij} - \frac{2}{3}\delta_{ij}\varepsilon$:

$$\phi_{ij1} \cong -C_1\bar\rho\varepsilon a_{ij}$$

$$C_1 = 1 + 2.58AA_2^{\frac{1}{4}}\left\{1 - \exp\left[-(Re_T/150)^2\right]\right\} \tag{17}$$

The rapid pressure–strain part was used to control separation. Careful observation of existing experimental data[46–48] and computational results with the Launder–Shima model[12] shows that in the separated flow region $A \to 1$. This observation was used in the modeling to obtain a better prediction of separated flow regions (invariably underpredicted by the Launder–Shima[30] model $C_2[A, Re_T]$). The original form of the Launder–Shima[30] model was, nonetheless, retained in the near-wall region, where it gives the correct near-wall behavior of the Reynolds stresses. For this reason, the coefficient of the isotropization of production closure used follows the Launder–Shima closure in the range $A \in [0, 0.55]$ and is then sharply raised. Because $A > 0.55$ in the log-law region, this modification is active at the outer part of boundary layers and in the separation region:

$$\phi_{ij2} \cong -C_2\left(P_{ij} - \tfrac{1}{3}\delta_{ij}P_{\ell\ell}\right) \tag{18}$$

$$C_2 = \min[1, 0.75 + 1.3\max[0, A - 0.55]]$$

$$\times A^{[\max(0.25, 0.5 - 1.3\max[0, A - 0.55])]}[1 - \max(0, 1 - Re_T/50)] \tag{19}$$

Table 1 Computational grids used[a]

Case	N_i	N_j	N_k	r_j	r_k	y_w^+	z_w^+	L_x, m	L_y, m	L_z, m
Boundary layer $M_e = 0.22$	401	201	——	1.081	——	0.46	——	3.000	0.152	——
Boundary layer $M_e = 0.60$	401	201	——	1.090	——	0.46	——	3.000	0.152	——
Compression ramp	401	201	——	1.100	——	0.50	——	0.170	0.200	——
Three-dimensional swept bump	265	161	181	1.107	1.095	0.75	0.75	0.800	0.100	0.1213

[a]Grid directions: i, j, k; number of points: N_i, N_j, N_k; geometric progression ratio: r_j, r_k; length: L_x, L_y, L_z.

Table 2 Inflow and wall boundary conditions used

Case	δ_∞, m	M_∞	T_{u_∞}, %	p_{t_∞}, Pa	T_{t_∞}, K	T_w, K	q_w, W · m^{-2}
Boundary layer $M_e = 0.22$	0.0250	0.22	1	101,325	288	——	0
Boundary layer $M_e = 0.60$	0.0250	0.60	1	101,325	288	——	0
Compression ramp	0.0280	2.84	1	665,000	250	260	——
Three-dimensional swept bump	0.0005	0.57	1	92,000	300	——	0

Echo Terms

During the model development extensive tests were run, including the suggestions by Launder and Li,[14] Craft[25] and Batten et al.[26] It was found that these closures, associated with a cubic pressure–strain model, did not perform satisfactorily in separated flows, in part due to numerical instabilities. One conclusion that seemed to come out of these tests was that echo terms were necessary both for the slow and the rapid pressure–strain terms. Furthermore, the forms suggested by Craft[25] for replacing the normal to the wall and the distance to the wall were incompatible with the ϕ_{ij1} and ϕ_{ij2} closure used in the present work.

The echo terms are computed in the usual way[49]:

$$\phi_{ij1}^w \cong C_1^w(\varepsilon/k)\left[\bar{\rho}\widetilde{u_k''u_m''}n_k n_m\delta_{ij} - \tfrac{3}{2}\bar{\rho}\widetilde{u_k''u_i''}n_k n_j - \tfrac{3}{2}\bar{\rho}\widetilde{u_k''u_j''}n_k n_i\right]$$

$$\phi_{ij2}^w \cong C_2^w\left[\phi_{km2}n_k n_m\delta_{ij} - \tfrac{3}{2}\phi_{ik2}n_k n_j - \tfrac{3}{2}\phi_{jk2}n_k n_i\right] \quad (20)$$

where $\boldsymbol{e}_n = n_i\boldsymbol{e}_i$ is the unit pseudonormal direction. The effect of the distance from the wall is included in the functions C_1^w and C_2^w.

To construct the wall reflection echo terms the normal to the wall direction is approximated by the gradient of a function of the turbulence length scale ℓ_T. To correct the problem of the maximum ℓ_T location in the boundary layer,[14] the following gradient is used:

$$\boldsymbol{e}_n = n_i\boldsymbol{e}_i = \frac{\text{grad}\ell_n}{\|\text{grad}\ell_n\|}, \qquad \ell_n = \frac{\ell_T\{1-\exp[-(Re_T/30)]\}}{1+2\sqrt{A_2}+2A^{16}}$$

$$\ell_T = \frac{k^{\frac{3}{2}}}{\varepsilon} \quad (21)$$

Adding (A^{16}) improves the approximation of the normal to the wall direction at the shock-wave foot. This form of the unit pseudonormal gives satisfactory results not only for simple boundary-layer flows but also at solid corners, as shown in the validation section. The coefficients C_1^w and C_2^w are made proportional to a power of the turbulence length-scale gradient, so that they will vanish in homogeneous flow:

$$C_1^w = 0.83\left[1-\tfrac{2}{3}(C_1-1)\right]\left\|\text{grad}\ell_1^w\right\|$$

$$\ell_1^w = \frac{\ell_T\{1-\exp[-(Re_T/30)]\}}{1+2A_2^{0.8}}$$

$$C_2^w = \max\left[\frac{2}{3}-\frac{1}{6C_2}, 0\right]\left\|\text{grad}\ell_2^w\right\|$$

$$\ell_2^w = \frac{\ell_T\{1-\exp[-(Re_T/30)]\}}{1+1.8A_2^{\max(0.6,A)}} \quad (22)$$

These forms were obtained after extensive testing over a wide range of configurations and are of course dependent on the closure used for ϕ_{ij1} and ϕ_{ij2}.

Model Validation

Computational Methods

The computational results were obtained using the numerical method for the three-dimensional compressible Navier–Stokes equations with RSM closure developed by Gerolymos and Vallet,[12] Gerolymos et al.,[13] and Gerolymos and Vallet.[40] The equations are discretized in space using a third-order upwind-biased flux-vector-splitting method and integrated in time using an implicit first-order method. A Courant–Friedrichs–Lewy number = 20 time step was used, based on a combined convective–diffusive stability time step.[12] The computational grids used are summarized in Table 1, and the boundary-conditions applied are given in Table 2 (for subsonic inflow M_∞ is of course not a boundary condition, but a result of the computations). In all cases grid dependence of results was carefully studied and eliminated as far as possible (Table 1).

Flat-Plate Boundary Layer

The model was then validated against experimental data for compressible subsonic boundary-layer flows, at near-zero pressure-gradient conditions.[50] Computations are compared with measurements at $M_e = 0.22$ and 0.6. Both the upper and lower wind-tunnel walls were included in the computations (height $L_y = 0.152$ m), which used a 401×201 grid (Table 1) for a streamwise length of $L_x = 3$ m. Inflow boundary conditions (Table 2) were based on measurements. The boundary-layer thickness at inflow δ_∞ was chosen to obtain the experimental momentum thickness Reynolds number Re_θ in the middle part of the computational domain well away from inflow and outflow and eventual contaminating influence from the boundary conditions. The results show satisfactory agreement with measurements (Fig. 1). Computed nondimensional mass-flux profiles are in good agreement with measurements (Fig. 1). For both Mach numbers a log-law region is obtained with von Kàrmàn constant $\kappa_{VK} = 0.435$, but with different ordinates at $y^+ = 1$. Agreement between computed and measured Reynolds stresses is quite good (Fig. 1) with the exception of the $\widetilde{v''v''}$ level, which is higher in the experiments. Nonetheless, the computed $\widetilde{v''v''}$ is nearer the generally accepted incompressible flow structure.[51] In conclusion, the present pseudonormal technique yields very satisfactory results for these near-zero pressure-gradient boundary-layer flows.

Oblique Shock-Wave at Compression Corner

To evaluate the performance of the present model in separated flows, computations were run for the interaction of a turbulent boundary layer with an oblique shock wave ($M_\infty = 2.84$) at a 24-deg compression corner (Fig. 2). This configuration is very well adapted to the evaluation of the model capability to predict correctly separation because the upstream influence indicated in the wall-pressure distribution (Fig. 3) is directly related to the size of the boundary-layer separation bubble.[52] Measurements were obtained for this configuration by various authors.[53–57] These measurements[56] were all obtained, over the years, on the same experimental setup and may

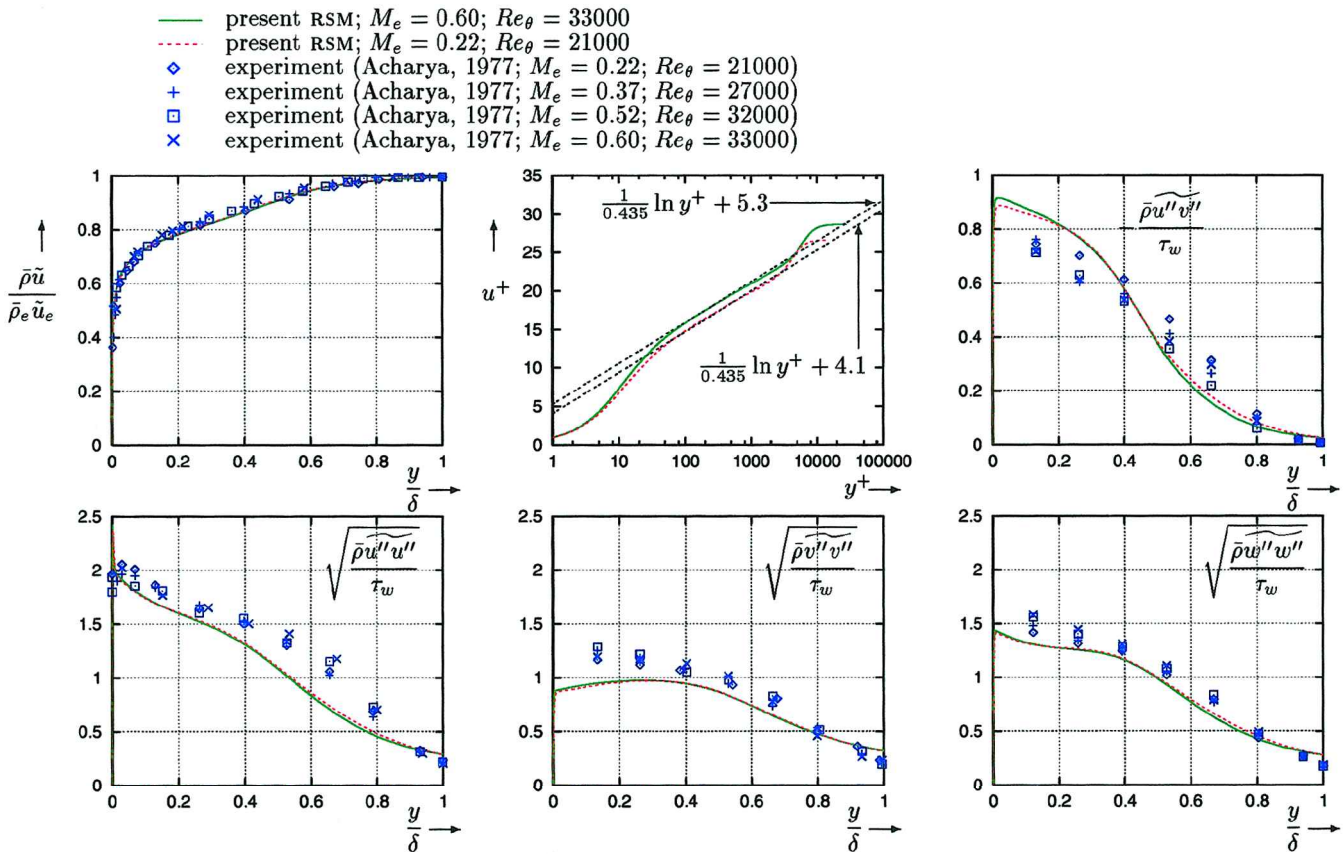

Fig. 1 Mean mass flux $\bar{\rho}\tilde{u}$, logarithmic law u^+, and Reynolds stresses for near-zero pressure-gradient boundary-layer flow (comparison with measurements of Acharya[50] at $M_e = 0.22$ and $Re_\theta = 2.1 \times 10^4$, and at $M_e = 0.6$ and $Re_\theta = 3.3 \times 10^4$).

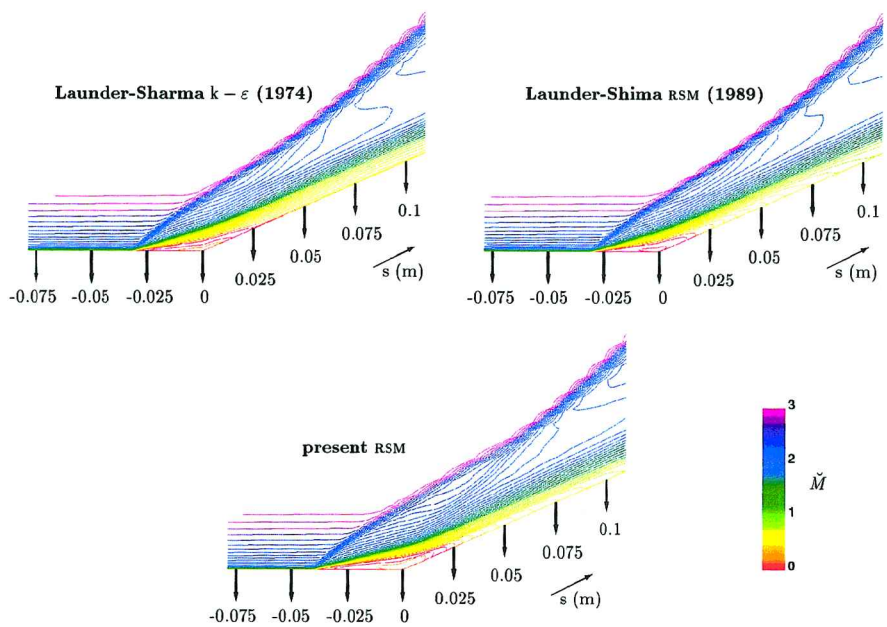

Fig. 2 Levels of Mach number $\check{M}$ for the 24-deg compression ramp of Settles et al.[53] at $M_\infty = 2.84$ (zoom of the corner region).

be taken as representing the experimental accuracy for this difficult configuration exhibiting a high level of shock-wave unsteadiness.[55] It is noticeable that, whereas important scatter is observed downstream of the interaction, all of the experimental data predict the same upstream influence due to the shock-wave/boundary-layer interaction at the corner (Fig. 3). Computations were run both with the Launder–Shima RSM,[30] as modified by Gerolymos and Vallet,[12] and with the present RSM model. Computations using the Launder–Sharma[31] k–ε model were run as well. A 401×201 computational grid was used (Table 1) which discretized both the ramp and the upper wind-tunnel wall ($L_y = 0.2$ m) for a length $L_x = 0.17$ m (Table 2).

Boundary conditions (Table 2) were based on the experimental data.[53–57] Following the tabulation of experimental data given by Fernholz et al.,[57] the wall temperature was fixed at $T_w = 260$ K, that is, about 10% higher than the adiabatic wall recovery temperature. The computed boundary-layer thickness at the beginning of the interaction is $\delta_0 = 0.023$ m, in accordance with the measurements.[53]

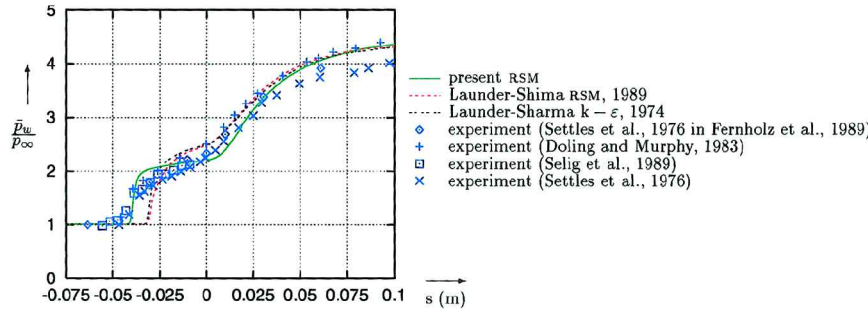

Fig. 3 Comparison of computed wall pressures $\bar{p}_w$ as a function of the curvilinear coordinate (s), with measurements[56] for the 24-deg compression ramp of Settles et al.[53] at $M_\infty = 2.84$ (zoom of the corner region).

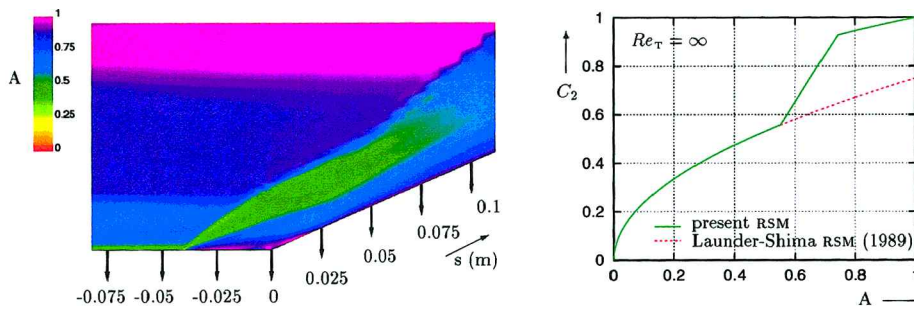

Fig. 4 Levels of A obtained using the present RSM model for the 24-deg compression ramp of Settles et al.[53] at $M_\infty = 2.84$ (zoom of the corner region) and plot of $C_2(A, Re_T = \infty)$ as a function of the anisotropy-tensor flatness parameter A.

The computed Mach-number plots (Fig. 2) obtained using the three models show that the present RSM model predicts a larger separation zone, and, as a result, a marked λ-shock structure, contrary to the two other models.

Comparison of computed wall-pressures $\bar{p}_w$ with measurements shows that the present RSM model correctly predicts the length of upstream influence of the ramp due to the shock-wave/boundary-layer interaction (Fig. 3), in contrast with the two other models: Both the Launder–Sharma k–ε model[31] and the Launder–Shima RSM model[30] give similar results that underpredict the upstream influence of the interaction. The obtained improvement is mainly due to the new form of C_2 used in the present model, as shown by examining (Fig. 4) the level plots of the flatness parameter A and the function $C_2(A, Re_T = \infty)$. Indeed, A varies monotonically from 0 at the wall to 1 outside of the boundary layer in the zero pressure-gradient region upstream of the interaction, whereas it takes high (near-unity) values in the separated flow region exhibiting a double-peak structure in the normal to the wall direction. Note also the wave-like region, clearly marked by $A \sim 0.5$, above the separated zone. The proposed modification of C_2 is active in the separated flow region and substantially improves the agreement with measurements compared to the standard C_2 function used in the Launder–Shima model.[30] Note, however, that the computed wall friction, after reattachment, approaches the equilibrium value too fast, a problem also observed by Rizzetta[58] using various explicit algebraic RSM closures. This drawback of the model may be attributed to the baseline equation used for ε (Refs. 32–34), but further research is needed to clarify this point (Wilcox[59] suggests that the use of multiscale models is necessary to obtain the correct wall-friction distribution).

Délery Three-Dimensional Nozzle

Finally, to demonstrate the ability of the present model to predict complex three-dimensional flows, results are presented for the Délery three-dimensional nozzle, which is a nozzle of rectangular cross section fitted with a three-dimensional swept bump at the lower wall (see Ref. 47). This configuration includes a shock wave whose upstream Mach-number is ~1.5 at the far wall and ~1.8 at the near wall, resulting in an important three-dimensional separation region in the near-wall vicinity (Fig. 5). The large separation is clearly seen as a low-speed region in the iso-Machs (Fig. 5). This zone has an important lateral extent (y-wise and z-wise) covering almost one-half of the channel and extends far downstream, up to the second throat used to position the shock wave.

Results obtained using the Launder–Shima RSM model[30] (also see Ref. 12) and the Launder–Sharma k–ε model[31] have been presented by Gerolymos and Vallet[12] and showed satisfactory agreement with measurements, but improvements were possible in the region of large separation. Comparison of computed skin-friction lines on the lower wall (Fig. 5) shows that the present model substantially improves the three-dimensional separation structure compared to the Launder–Shima model (see Ref. 12). Indeed measurements[47] (photographs of colored viscous coating at the wall) show that the separation at the lower wall is delimited by a separation line S_1 intersecting the near wall at point C_1 and terminating at focal point F_1 around which a three-dimensional $(\tilde{u}$–$\tilde{w})$ separation bubble is organized. The separation region is delimited downstream by the reattachment line S_2 intersecting the lower wall at point C_2 (Fig. 5).

The Launder–Shima RSM closure[30] (also see Ref. 12) does not predict the wall-friction lines pattern correctly. Although the separation line S_1 (point C_1) is correctly located (due to the correct prediction of the position of the shock wave, which is responsible for the separation) the focal point F_1 is too far downstream and too near the wall (too far from nozzle midspan). Furthermore, the form of the recirculation region is too elongated, and the reattachement line intercept C_2 is too far downstream. The present RSM model substantially improves agreement with measurements. Both the separation line S_1 and the focal point F_1 are correctly captured. The reattachement line intercept C_2 is quite well predicted. This important improvement in separated flow structure is associated with a better prediction of streamwise $\tilde{u}$ and crossflow $\tilde{w}$ velocity profiles (Fig. 6). Indeed the separated region is characterized by a cross-flow wall jet (high $\tilde{w}$ near the wall) feeding the recirculation zone and almost inhibiting (in the measurements) negative $\tilde{u}$ velocities. The present RSM model predicts a stronger $\tilde{w}$ wall jet (Fig. 6), and in this way improves the agreement with measurements. The improvement is partly attributed to the use of pseudonormals instead of geometric normals. Pseudonormals behave correctly at solid corners (Fig. 7), thus automatically lifting the ambiguity in geometrically defining a normal to the wall direction and a distance from the wall (or the eventual use of separate echo terms for each wall[12]).

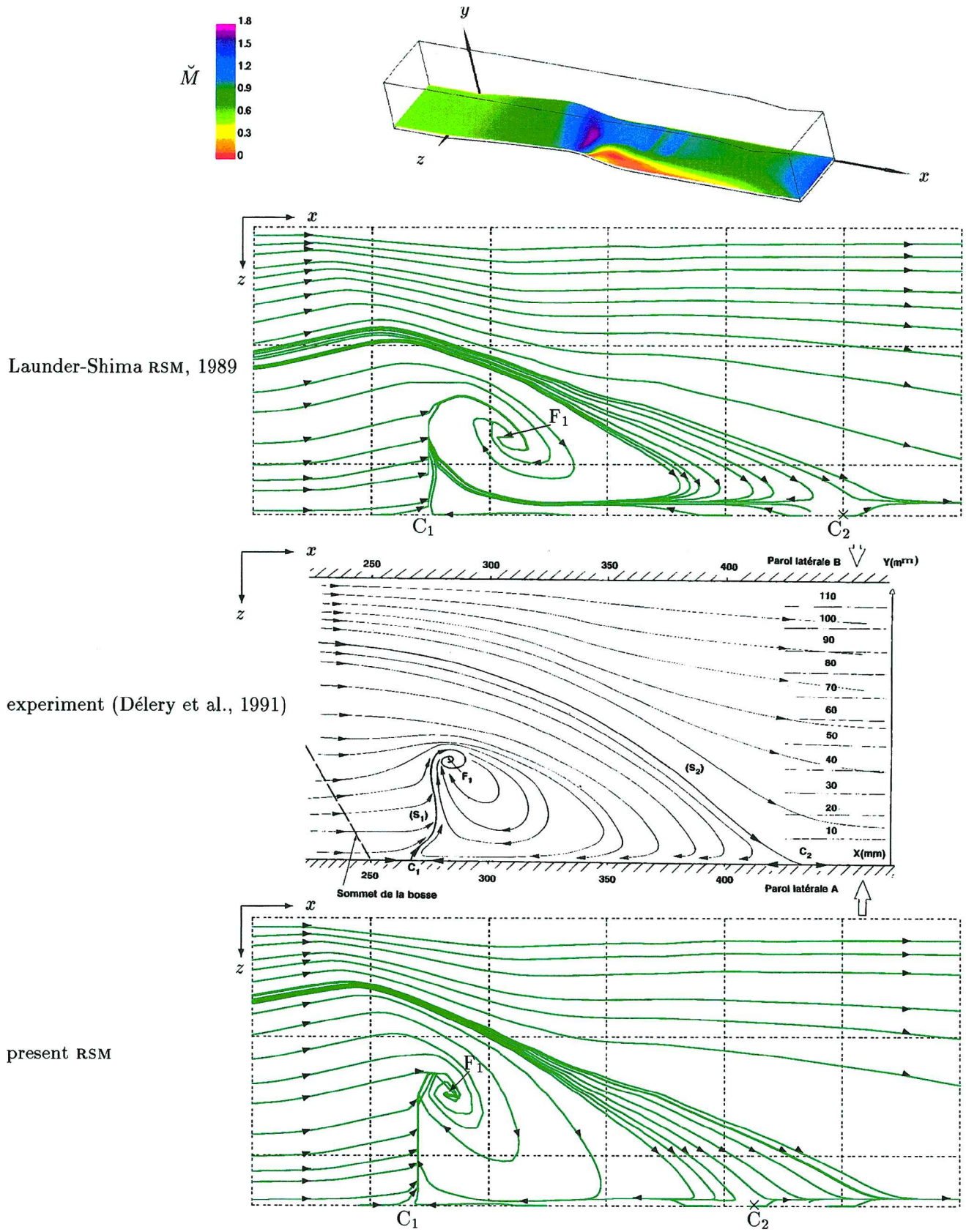

Fig. 5 Level of Mach number $\breve{M}$ for the Délery three-dimensional nozzle (see Ref. 47) near the lower wall obtained using the present RSM model and comparison of computed skin-friction lines on the lower wall (using the present RSM model and the Launder–Shima RSM model[30] with measurements. (The experimental reference frame was $X = x$, $Y = 0.1213 - z$, $Z = y$.)

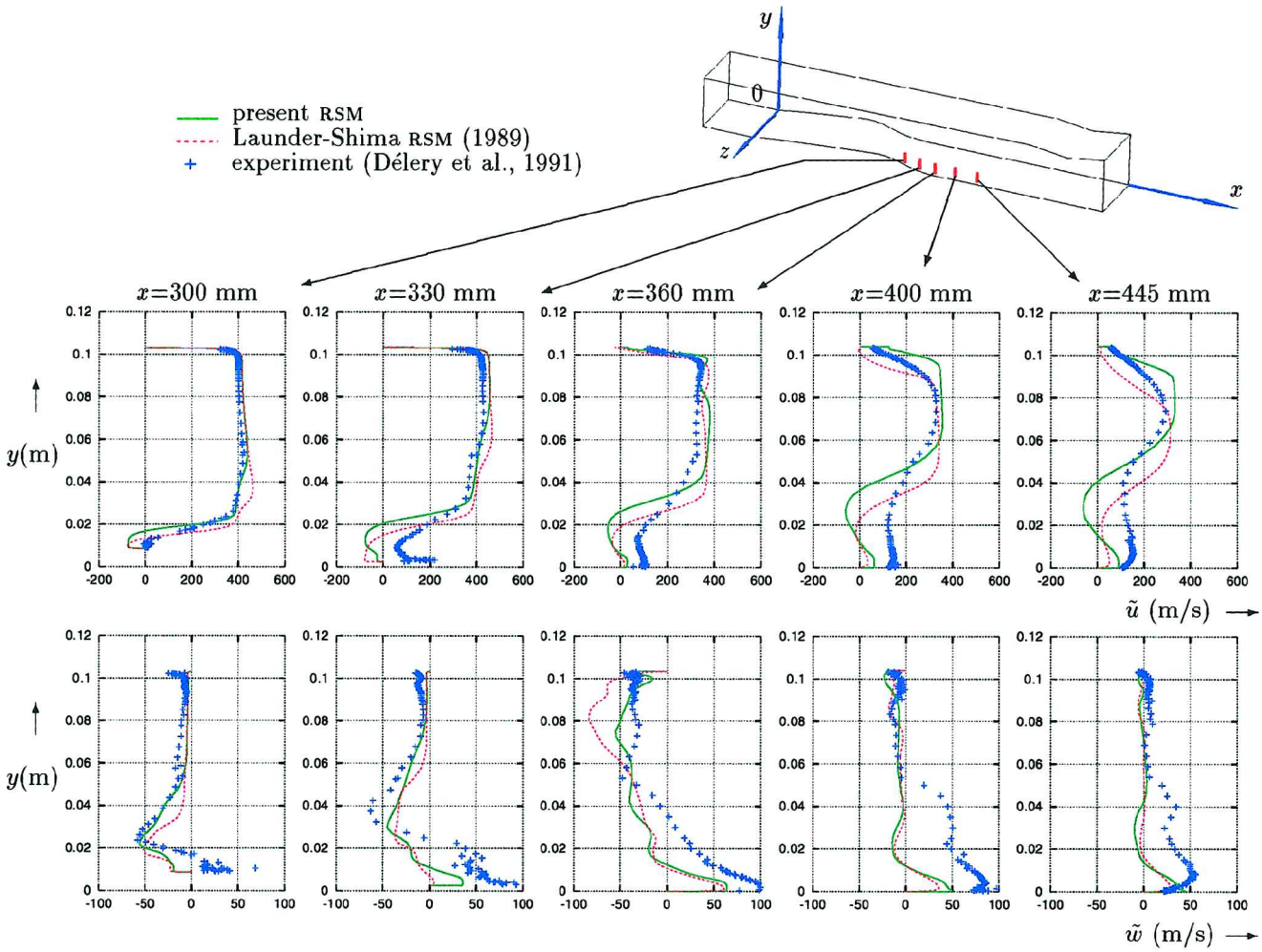

Fig. 6 Comparison of computed $\tilde{u}$ (x-wise) and $\tilde{w}$ (z-wise) velocity profiles [using the present RSM model and the Launder–Shima RSM model[30] (also see Ref. 12)] with measurements for the Délery three-dimensional nozzle (see Ref. 47) at six x-wise stations, in the separated flow region ($z = 0.1113$ m).

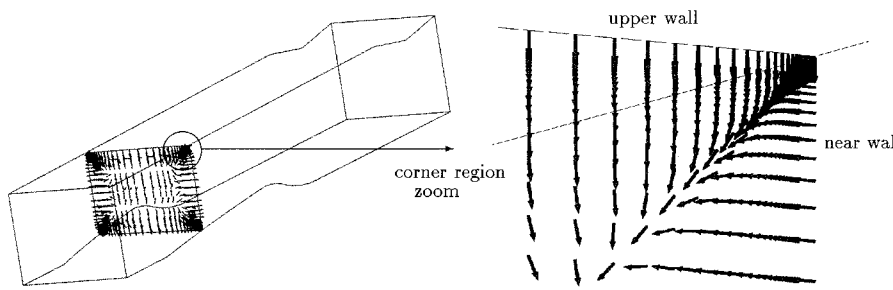

Fig. 7 Unit pseudonormals of the present model at a solid corner for the Délery three-dimensional nozzle (see Ref. 47).

The agreement is less satisfactory in the outer part of the boundary layer.

The model has been extended to rotating flows and has been validated by comparison with measurements for three-dimensional transonic turbomachinery flows.[60,61]

Conclusions

In the present work, a wall-normal-free, near-wall RSM model was developed and validated. The model does not require the geometric definition of the normal to the wall direction and of the distance to the wall, which are instead replaced by functions of the gradients of functions of the turbulence length scale and of the anisotropy tensor invariants. This makes the use of the model in complex three-dimensional geometries quite straightforward.

The model gives very satisfactory results for boundary-layer flows, demonstrating the capability of the wall-normal-free formulation to mimic the wall-echo effects correctly. The formulation used is based on a quasi-linear ϕ_{ij} closure, with pseudonormal-based echo terms. These two choices substantially enhance the model robustness and ensure numerical convergence for complex flows.

Comparison with experimental measurements for two- and three-dimensional shock-wave/boundary-layer interactions show that the present RSM model substantially improves the prediction of separation when compared to k–ε or other RSM closures. This improvement concerns both the extent and the structure of the separated flow region. The excellent agreement of skin-friction lines topology with measurements is partly attributed to the use of pseudonormals instead of geometric normals that are ambiguous at solid corners.

The resulting model is easy to code (compared to cubic ϕ_{ij} closures) and has been successfully applied to a number of complex (and numerically difficult) flows, giving results consistently better than previous closures. Nonetheless, the authors consider that

this is a baseline model, of good engineering accuracy, that can be further improved, by modifying the dissipation equation, by including a model for pressure diffusion, and by further optimizing the functional dependence of the quasi-linear pressure–strain closures coefficients on the anisotropy-tensorinvariants. These modeling additions are hoped to correct the two known drawbacks of the model, that is, the too rapid return of skin friction to equilibrium values after reattachment and the behavior of the outer part of the boundary layer in the reattachment and relaxation regions.

Acknowledgments

The computations presented in this work were run at the Institut pour le Développement des Ressources en Informatique Scientifique, where computer resources were made available by the Comité Scientifique. The authors wish to thank J. M. Délery for providing his experimental data and discussing the results. Authors are listed alphabetically.

References

[1]Johnston, J. P., Halleen, R. M., and Lezius, D. K., "Effects of Spanwise Rotation on the Structure of 2-D Fully Developed Turbulent Channel Flow," *Journal of Fluid Mechanics*, Vol. 56, 1972, pp. 533–557.

[2]Lakshminarayana, B., "Turbulence Modeling for Complex Shear Flows," *AIAA Journal*, Vol. 24, No. 12, 1986, pp. 1900–1917.

[3]Gessner, F. B., and Emery, A. F., "The Numerical Prediction of Developing Turbulent Flow in Rectangular Ducts," *Journal of Fluids Engineering*, Vol. 103, Sept. 1981, pp. 445–455.

[4]Davis, D. O., Gessner, F. B., and Kerlick, G. D., "Experimental and Numerical Investigation of Supersonic Turbulent Flow through a Square Duct," *AIAA Journal*, Vol. 24, No. 9, 1986, pp. 1508–1515.

[5]Davis, D. O., and Gessner, F. B., "Experimental Investigation of Turbulent Flow through a Circular to Rectangular Duct," *AIAA Journal*, Vol. 30, No. 2, 1992, pp. 367–375.

[6]Wellborn, S. R., Reichert, B. A., and Okiishi, T. H., "Study of the Compressible Flow in a Diffusing S-Duct," *Journal of Propulsion and Power*, Vol. 10, No. 5, 1994, pp. 668–675.

[7]Hanjalić, K., and Launder, B. E., "Contribution Towards a Reynolds-Stress Closure for Low-Reynolds-Number Turbulence," *Journal of Fluid Mechanics*, Vol. 74, 1976, pp. 593–610.

[8]Launder, B. E., "Numerical Computation of Convective Heat Transfer in Complex Turbulent Flows: Time to Abandon Wall-Functions?," *International Journal of Heat and Mass Transfer*, Vol. 27, No. 9, 1984, pp. 1485–1491.

[9]Launder, B. E., "Second-Moment Closure: Present...and Future?," *International Journal of Heat and Fluid Flow*, Vol. 10, No. 4, 1989, pp. 282–300.

[10]So, R. M. C., Lai, Y. G., Zhang, H. S., and Hwang, B. C., "Second-Order Near-Wall Turbulence Closures: A Review," *AIAA Journal*, Vol. 29, No. 11, 1991, pp. 1819–1835.

[11]Hanjalić, K., "Advanced Turbulence Closure Models: A View of Current Status and Future Prospects," *International Journal of Heat and Fluid Flow*, Vol. 15, No. 3, 1994, pp. 178–203.

[12]Gerolymos, G. A., and Vallet, I., "Near-Wall Reynolds-Stress Three-Dimensional Transonic Flow Computation," *AIAA Journal*, Vol. 35, No. 2, 1997, pp. 228–236.

[13]Gerolymos, G. A.,Tsanga, G., and Vallet, I., "Near-Wall k–ε Computation of Transonic Turbomachinery Flows with Tip Clearance," *AIAA Journal*, Vol. 36, No. 10, 1998, pp. 1769–1777.

[14]Launder, B. E., and Li, S. P., "On the Elimination of Wall-Topography Parameters from 2-Moment Closure," *Physics of Fluids*, Vol. 6, No. 2, 1994, pp. 999–1006.

[15]Durbin, P. A., "Near-Wall Turbulence Closure Modeling without Damping Functions," *Theoretical Computational Fluid Dynamics,*, Vol. 3, 1991, pp. 1–13.

[16]Durbin, P. A., "A Reynolds-Stress Model for Near-Wall Turbulence," *Journal of Fluid Mechanics*, Vol. 249, 1991, pp. 465–498.

[17]Pettersson, B. A., Andersson, H. I., and Brunvoll, A. S., "Modeling Near-Wall Effects in Axially Rotating Pipe Flow by Elliptic Relaxation," *AIAA Journal*, Vol. 36, No. 7, 1998, pp. 1164–1170.

[18]Djenidi, L., and Antonia, R. A., "Modeling of the Reynolds-Stress Transport Equation," *AIAA Journal*, Vol. 35, No. 3, 1997, pp. 450–455.

[19]So, R. M. C., and Yuan, S. P., "A Geometry Independent Near-Wall Reynolds-Stress Closure," *International Journal of Engineering Science*, Vol. 37, 1999, pp. 33–57.

[20]So, R. M. C., and Yuan, S. P., "Near-Wall 2-Equation and Reynolds-Stress Modeling of Backstep Flow," *International Journal of Engineering Science*, Vol. 36, No. 3, 1998, pp. 283–298.

[21]Shima, N., "Low-Reynolds-Number Second-Moment Closure without Wall-Reflection Redistribution Terms," *International Journal of Heat and Fluid Flow*, Vol. 19, 1998, pp. 549–555.

[22]Lumley, J. L., "Computational Modeling of Turbulent Flows," *Advances in Applied Mechanics*, Vol. 18, 1978, pp. 123–176.

[23]Bradshaw, P., Mansour, N. N., and Piomelli, U., "On Local Approximations of the Pressure–Strain Term in Turbulence Models," Center for Turbulence Research, Proceedings of the Summer Program Stanford Univ., Stanford, CA, 1987.

[24]Craft, T. J., Launder, B. E., and Suga, K., "Prediction of Turbulent Transitional Phenomena with a Nonlinear Eddy-Viscosity Model," *International Journal of Heat and Fluid Flow*, Vol. 18, No. 1, 1997, pp. 15–28.

[25]Craft, T. J., "Developments in a Low-Reynolds-Number Second-Moment Closure and its Applicatin to Separating and Reattaching Flows," *International Journal of Heat and Fluid Flow*, Vol. 19, 1998, pp. 541–548.

[26]Batten, P., Craft, T. J., Leschziner, M. A., and Loyau, H., "Reynolds-Stress-Transport Modeling for Compressible Aerodynamics Applications," *AIAA Journal*, Vol. 37, No. 7, 1999, pp. 785–797.

[27]Sommer, T. P., So, R. M. C., and Zhang H. S., "Near-Wall Variable-Prandtl-Number Turbulence Model for Compressible Flows," *AIAA Journal*, Vol. 31, No. 1, 1993, pp. 27–35.

[28]Sommer, T. P., So, R. M. C., and Zhang H. S., "Supersonic Flow Calculations using a Reynolds-Stress and a Thermal Eddy Diffusivity Turbulence Model," *Journal of Fluids Engineering*, Vol. 116, Sept. 1994, pp. 469–476.

[29]Ladeinde, F., "Supersonic Flux-Split Procedure for Second-Moments of Turbulence," *AIAA Journal*, Vol. 33, No. 7, 1995, pp. 1185–1195.

[30]Launder, B. E., and Shima, N., "Second-Moment Closure for the Near-Wall Sublayer: Development and Application," *AIAA Journal*, Vol. 27, No. 10, 1989, pp. 1319–1325.

[31]Launder, B. E., and Sharma, B. I., "Application of the Energy Dissipation Model of Turbulence to the Calculation of Flows near a Spinning Disk," *Letters in Heat and Mass Transfer*, Vol. 1, 1974, pp. 131–138.

[32]Hanjalić, K., and Jakirlić, S., "A Model of Stress Dissipation in Second-Moment Closures," *Applied Scientific Research*, Vol. 51, 1993, pp. 513–518.

[33]Hanjalić, K., and Jakirlić, S., "Contribution toward the Second-Moment Closure Modelling of Separating Turbulent Flows," *Computers and Fluids Journal*, Vol. 27, No. 2, 1998, pp. 137–156.

[34]Hanjalić, K., Hadžić, I., and Jakirlić, S., "Modeling Turbulent Wall Flows Subjected to Strong Pressure Variations," *Journal of Fluids Engineering*, Vol. 121, March 1999, pp. 57–64.

[35]Sotiropoulos, F., and Patel, V. C., "Prediction of Turbulent Flow Through a Transition Duct Using a Second-Moment Closure," *AIAA Journal*, Vol. 32, No. 11, 1994, pp. 2194–2204.

[36]Sotiropoulos, F., and Patel, V. C., "Application of Reynolds-Stress Transport Models to Stern and Wake Flows," *Journal of Ship Research*, Vol. 39, No. 4, 1995, pp. 263–283.

[37]Smits, A. J., and Dussauge, J. P., *Turbulent Shear Layers in Supersonic Flow*, AIP Press, Woodbury, NY, 1996.

[38]Gerolymos, G. A., "Implicit Multiple Grid Solution of the Compressible Navier–Stokes Equations using k–ε Closure," *AIAA Journal*, Vol. 28, No. 10, 1990, pp. 1707–1717.

[39]Vandromme, D., and Ha Minh, H., "About the Coupling of Turbulence Closure Models with Averaged Navier–Stokes Equations," *Journal of Computational Physics*, Vol. 65, 1986, pp. 386–409.

[40]Gerolymos, G. A., and Vallet, I., "Implicit Computation of the Three-Dimensional Compressible Navier–Stokes Equations using k–ε Turbulence Closure," *AIAA Journal*, Vol. 34, No. 7, 1996, pp. 1321–1330.

[41]Sarkar, S., and Lakshmanan, B., "Application of a Reynolds-Stress Turbulence Model to the Compressible Shear Layer," *AIAA Journal*, Vol. 29, No. 5, 1991, pp. 743–749.

[42]Sarkar, S., Erlebacher, G., Hussaini, M. Y., and Kreiss, H. O., "The Analysis and Modelling of Dilatational Terms in Compressible Turbulence," *Journal of Fluid Mechanics*, Vol. 227, 1991, pp. 473–493.

[43]Launder, B. E., Reece, G. J., and Rodi, W., "Progress in the Development of a Reynolds-Stress Turbulence Closure," *Journal of Fluid Mechanics*, Vol. 68, 1975, pp. 537–566.

[44]Hanjalić, K., and Launder, B. E., "A Reynolds Stress Model of Turbulence and its Application to Thin Shear Flows," *Journal of Fluid Mechanics*, Vol. 52, 1972, pp. 609–638.

[45]Daly, B. J., and Harlow, F. H., "Transport Equations in Turbulence," *Physics of Fluids*, Vol. 13, No. 11, 1970, pp. 2634–2649.

[46]Benay, R., Délery, J. M., and Pot, T., "Analyse Expérimentale de l'Ecoulement dans un Canal Transsonique 3-D," *Recherche Aérospatiale*, Vol. 1986, No. 6, 1986, pp. 399–414.

[47]Pot, T., Délery, J. M., and Quelin, C., "Interactions Onde-de-Choc/Couche-Limite dans un Canal Transsonique 3-D," ONERA, Rapport Technique ONERA 92-7078-AY-116-A, Feb. 1991.

[48]Cahen, J., Couailler, V., Délery, J. M., and Pot, T., "Validation of Code using Turbulence Model Applied to Three-Dimensional Transonic Channel," *AIAA Journal*, Vol. 33, No. 4, 1995, pp. 671–679.

[49]Gibson, M. M., and Launder, B. E., "Ground Effects on Pressure Fluctuations in the Atmospheric Boundary Layer," *Journal of Fluid Mechanics*, Vol. 86, 1978, pp. 491–511.

[50]Acharya, M., "Effects of Compressibility on Boundary-Layer Turbulence," *AIAA Journal*, Vol. 15, No. 3, 1977, pp. 303, 304; also AIAA Paper 76-334, 1976.

[51]Klebanoff, P. S., "Characteristics of Turbulence in a Boundary-Layer with Zero Pressure Gradient," NACA Rept. 1247, 1955.

[52]Délery, J. M., "Shock-Wave/Turbulent-Boundary-LayerInteraction and its Control," *Progress Aerospace Sciences*, Vol. 22, 1985, pp. 209–280.

[53]Settles, G. S., Vas, I. E., and Bogdonoff, S. M., "Details of a Shock-Separated Turbulent Boundary Layer at a Compression Corner," *AIAA Journal*, Vol. 14, No. 12, 1976, pp. 1709–1715.

[54]Settles, G. S., Fitzpatrick, T. J., and Bogdonoff, S. M., "Detailed Study of Attached and Separated Compression Corner Flowfields in High Reynolds Number Supersonic Flow," *AIAA Journal*, Vol. 17, No. 6, 1979, pp. 579–585.

[55]Dolling, D. S., and Murphy, M. T., "Unsteadiness of the Separation Shock-Wave Structure in a Supersonic Compression Ramp Flowfield," *AIAA Journal*, Vol. 21, No. 12, 1983, pp. 1628–1634.

[56]Sellig, M. S., Andreopoulos, J., Muck, K. C., Dussauge, J. P., and Smits, A. J., "Turbulence Structure in a Shock-Wave/Turbulent-Boundary-Layer Interaction," *AIAA Journal*, Vol. 27, No. 7, 1989, pp. 862–869.

[57]Fernholz, H. H., Finley, P. J., Dussauge, J. P., and Smits, A. J., "A Survey of Measurements and Measuring Techniques in Rapidly Distorted Compressible Turbulent Boundary Layers," AGARDograph 315, 1989.

[58]Rizzetta, D. P., "Evaluation of Explicit Algebraic Reynolds-Stress Models for Separated Supersonic Flows," *AIAA Journal*, Vol. 36, No. 1, 1998, pp. 24–30.

[59]Wilcox, D. C., "Supersonic Compression-Corner Applications of a Multiscale Model for Turbulent Flows," *AIAA Journal*, Vol. 28, No. 7, 1990, pp. 1194–1198.

[60]Gerolymos, G. A., and Vallet, I., "Wall-Normal-Free Reynolds-Stress Model for Compressible Rotating Flows Applied to Turbomachinery," *AIAA Journal* (to be published).

[61]Gerolymos, G. A., Neubauer, J., Sharma, V. C., and Vallet, I., "Improved Prediction of Turbomachinery Flows using Near-Wall Reynolds-Stress Model," *Journal of Turbomachinery* (to be published); also ASME Paper 2001-GT-0196.

R. M. C. So
Associate Editor

Color reproductions courtesy of Université Pierre-et-Marie-Curie.